Letter

Tunable anti–parity-time-symmetric chaos in optomechanics

Feifan Huang,[*] Lei Chen,[*,†] Linwei Huang, Junhua Huang, Guishi Liu, Yaofei Chen, Yunhan Luo,[‡] and Zhe Chen
Guangdong Provincial Key Laboratory of Optical Fiber Sensing and Communications, College of Science and Technology, Jinan University, Guangzhou 510632, China
and Key Laboratory of Optoelectronic Information and Sensing Technologies of Guangdong Higher Education Institutes, Jinan University, Guangzhou 510632, China

(Received 29 May 2021; accepted 25 August 2021; published 7 September 2021)

The chaotic light source is one of the most crucial foundations in optical physics studies and photonic devices. The microcavity provides the predominant solution of compact chaotic light sources in integrated photonics. Still, its prefixed feature has severely ruled out access to tuning for meeting the ever-increasing demands of the general-purpose chaotic light source in engineering. Here we report a demonstration of a chaotic light source with a switchable bandpass–band-stop chaotic emission and tunable bandwidth in a spinning microcavity anti-parity-time (anti-$\mathcal{PT}$). system. In addition, the arrangement of anti-$\mathcal{PT}$ microcavity presents several phenomena such as loss-induced chaotic emission and two different chaotic emissions from one microcavity light source. Such advantages offer another possible way to advance multiplex photonic devices and on-chip chaotic light source fabrication. These results provide a promising approach for the tunable chaotic source and serve as tools for applications in secure communications, electromechanical switching, and exploring non-Hermitian physics.

DOI: 10.1103/PhysRevA.104.L031503

I. INTRODUCTION

Due to the strongly nonlinear interaction between radiation pressure and the mechanical mode in a microcavity, the optomechanical system (OMS) provides a golden opportunity to drive a mesoscopic system accessing classical and quantum dynamics [1–6]. For example, OMSs have been employed for the preparation of Schrödinger cat states [7,8], the generation of light-matter entanglement [9], the nonreciprocal phonon laser [10], and single-particle sensing [11,12]. More essentially, an OMS driven by a powerful laser can enter into a regime of self-induced oscillations, where the light-coupled mechanical gain overcomes the intrinsic mechanical loss. Upon further increasing the strength of the pump laser, chaotic dynamics emerges in both the optical and mechanical modes without external feedback or modulation [11,13]. The investigation of chaotic dynamics has opened up possibilities for discoveries and applications such as decoherence suppression [14], random number generation [15–17], secure communication [18], and broadband optical devices [19,20].

A tunable bandwidth or convertible bandpass–band-stop feature is desirable for most optical devices [21–23]. However, a microcavity transmission is difficult to tune because once the microcavities are fabricated, dynamically controlling their prefixed parameters usually relies on strongly nonlinear processes [24]. Thus, multiple-task nonlinear interaction has to generate a chaotic signal and tunes the microcavity resonance simultaneously, which poses a direct challenge in both theory and practical applications.

Since the dissipative terms were introduced into optics, the notion of non-Hermitian optics has attracted an enormous amount of attention. As the first notion introduced, parity-time ($\mathcal{PT}$) symmetry has produced extensive novel applications, such as $\mathcal{PT}$-symmetry-phonon lasers [25,26], reconfigurable chiral lasers [27], loss-induced lasers [28], and exception point enhanced gyroscopes [29]. Furthermore, the marriage of $\mathcal{PT}$ photonics and the OMS has demonstrated an ultralow chaos threshold [13]. However, an optical gain introduces noise from the heat reservoir, which may destroy the quantum coherence [30]. Therefore, an equivalent passive $\mathcal{PT}$-symmetric waveguide or microcavity pair was commonly used in the confirmation experiments [31]. Such a passive arrangement ignites the interest in another non-Hermitian Hamiltonian operator, called anti–parity-time symmetry [32].

Anti-$\mathcal{PT}$ symmetry in the microcavity system suggests that two optical modes with different resonances generate a dissipative coupling [33,34]. The uniqueness of the anti-$\mathcal{PT}$ symmetry provides a fruitful platform to study complex physical phenomena in the wave dynamics and diffusive system [35], including the exceptional-point enhanced Sagnac effect [36], anti–$\mathcal{PT}$-symmetric Berry phase [37], and resonant-tunable isolator [38]. Two typical schemes, i.e., the synthetic anti–$\mathcal{PT}$-symmetric microcavity [39] and spinning microcavity [40], are commonly used in the anti–$\mathcal{PT}$-involved confirmation experiments. Since the rotational speed is much easier to continuously tune *in situ* than the internal nonlinearity of materials, providing a different degree of freedom to tailor the spectrum [41], the spinning microcavity is widely used in the Sagnac effect induced slow light [42], ultrasensitive detection [40], synthetic gauge

[*]These authors contributed equally to this work.
[†]Corresponding author: chenlei@jnu.edu.cn
[‡]Corresponding author: yunhanluo@163.com

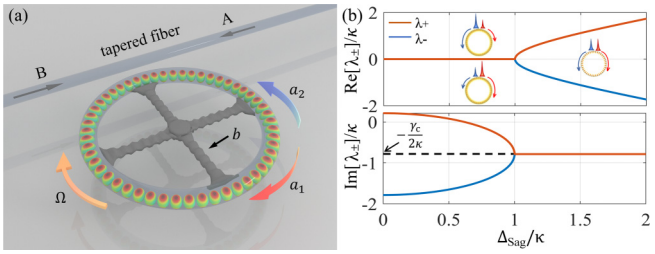

FIG. 1. (a) Realization of a spinning microcavity anti-$\mathcal{PT}$ OMS. The microcavity is driven by two lasers with the same angular frequency from ports A and B, generating the clockwise mode a_1, counterclockwise mode a_2, and mechanical mode b. The rotational speed of microcavity Ω adjusts the anti-$\mathcal{PT}$ symmetry [38], which induces two opposite angular frequency shifts on two optical modes. (b) Solutions of the real and imaginary parts of the eigenvalues λ_+ (top) and λ_- (bottom) in the absence of mechanical motion.

field [43], and nonreciprocal photon blockade [44–46]. The heuristic question of whether an anti-$\mathcal{PT}$ symmetry could tune the chaotic dynamics in different wavelengths and constitute a general-purpose chaotic light source, considering it couples two optical modes with different resonances, motivates us to study the spinning microcavity anti-$\mathcal{PT}$ system. More importantly, the uninvestigated crossover between the anti-$\mathcal{PT}$-symmetry theory and chaos in the OMS may substantially advance the fields of non-Hermitian physics and chaos in optics.

This study proposes a chaotic light source with a tunable bandwidth and switchable bandpass–band-stop feature in the spinning anti-$\mathcal{PT}$ OMS. In contrast to earlier chaotic light sources, the tunable rotational speed enables us to harness the anti-$\mathcal{PT}$ phase transition. It benefits from the proposed chaotic source being able to freely switch chaotic emission from bandpass to band stop in a tunable bandwidth. This advantage ultimately allows a single microcavity to generate two independent chaotic outputs and directly decreases the chaos threshold. In addition, another phenomenon, loss-induced chaos, was characterized in the proposed anti-$\mathcal{PT}$ system, which is different from the conventional mechanism of power-induced chaos, benefiting the microcavity fabrication in chaos generation. This chaos generation mechanism, providing a tunable scheme, is identified in the spinning anti-$\mathcal{PT}$ OMS.

II. THEORETICAL MODEL AND ANALYSIS

When an OMS couples to a spinning microcavity anti-$\mathcal{PT}$ system through the optical tunneling shown in Fig. 1(a), the system Hamiltonian can be described by [3,5,8]

$$H_{\rm sym} = H_{a\text{-}\mathcal{PT}} + H_m - i\hbar\Omega_d \sum_{i=1,2}(a_i^\dagger - a_i), \tag{1}$$

where $H_{a\text{-}\mathcal{PT}} = \hbar\Delta_+ a_1^\dagger a_1 - \hbar\Delta_- a_2^\dagger a_2 + i\hbar\kappa(a_1^\dagger a_2 + a_1 a_2^\dagger)$ and $H_m = \hbar\omega_m b^\dagger b - \hbar g(b^\dagger + b)\sum_{i=1,2} a_i^\dagger a_i$. The terms of a_i ($a_i^\dagger$) and b ($b^\dagger$) are the annihilation (creation) operators of the optical modes and mechanical mode, respectively. Here κ is the coupling between two cavity modes. The microcavity is driven with frequency ω_d and amplitude $\Omega_d = \sqrt{2P\gamma_c/\hbar\omega_d}$, with P denoting power and γ_c the decay rate of the microcavity. Further, Δ_+ and Δ_- are the detunings in a frame rotating with ω_d, i.e., $\Delta_\pm = \omega_c - \omega_d \pm \Delta_{\rm Sag}$, with ω_c the angular frequency of the microcavity and $\Delta_{\rm Sag}$ the angular frequency given by the spinning-induced Sagnac effect [38]. In addition, ω_m and g are the angular frequency of the mechanical mode and the coupling between the optical modes and the mechanical mode, respectively. Here we consider that the system Hamiltonian is composed of three parts: The first term on the right-hand in Eq. (1) characterizes the cavity modes a_i with resonance frequency $\Delta_\pm$ and the coupling between the cavity modes; the second term describes the mechanical mode b with resonance frequency ω_m and the interaction between the mechanical mode and cavity modes; the third term gives the input and output relations of the fiber taper coupled spinning microcavity. In the high-power situation, the interactions of the mechanical-cavity mode, the cavity-cavity mode, and the fiber taper and spinning microcavity have been validated experimentally [14].

To explore the chaotic dynamics of the spinning anti-$\mathcal{PT}$ microcavity system, we employed the semiclassical Langevin equations of motion. Furthermore, by defining the dimensionless position operator $x = (b^\dagger + b)/\sqrt{2}$ and momentum operators $p = i(b^\dagger - b)/\sqrt{2}$ of the mechanical mode, the master equation of the OMS can be described by [13]

$$\dot{x} = \omega_m p, \tag{2a}$$

$$\dot{p} = -\left(\frac{\gamma_m}{2}\right)p - \omega_m x + \sqrt{2}g\sum_{i=1,2}|a_i|^2, \tag{2b}$$

$$\dot{a}_1 = \left(-i\Delta_+ - \frac{\gamma_c}{2}\right)a_1 + \kappa a_2 + i\sqrt{2}g a_1 x - \Omega_d, \tag{2c}$$

$$\dot{a}_2 = (-i\Delta_- - \gamma_c/2)a_2 + \kappa a_1 + i\sqrt{2}g a_2 x - \Omega_d, \tag{2d}$$

where γ_m is the decay rate of the mechanical mode.

To better understand the spinning microcavity anti-$\mathcal{PT}$ system, we calculated the eigenvalues in the absence of mechanical motion and present their results in Fig. 1(b). For a low rotational speed ($\Delta_{\rm Sag}/\kappa < 1$), the eigenvalues preserve the anti-$\mathcal{PT}$ symmetry, having the same real part and different imaginary parts. This indicates that two eigenmodes possess the same resonance wavelength but different strengths for the clockwise and counterclockwise components. The anti–$\mathcal{PT}$-symmetric breaking occurs if the spinning is further enhanced ($\Delta_{\rm Sag}/\kappa > 1$), where the imaginary part coalesces, but the real part bifurcates. An interesting phenomenon is that the anti–$\mathcal{PT}$-symmetric phase in a low-rotational-speed regime allows the imaginary part to obtain a positive value rather than a usual negative value [34]. Generally, a positive imaginary part suggests that the light intensity obtains an optical gain. However, the spinning microcavity system is passive and therefore such an unusual feature offers intriguing chaotic dynamics.

Here we discuss the experimental feasibility. The spinning microcavity was recently manifested experimentally in an optical isolator [47], and several studies in sensing were developed using the spinning microcavity arrangement [38,40]. The present study is directly based on the first work on realizing anti-$\mathcal{PT}$ symmetry in a spinning cavity [38]. Based on the above pioneering studies, we select a fiber taper to guide light into the spinning microcavity

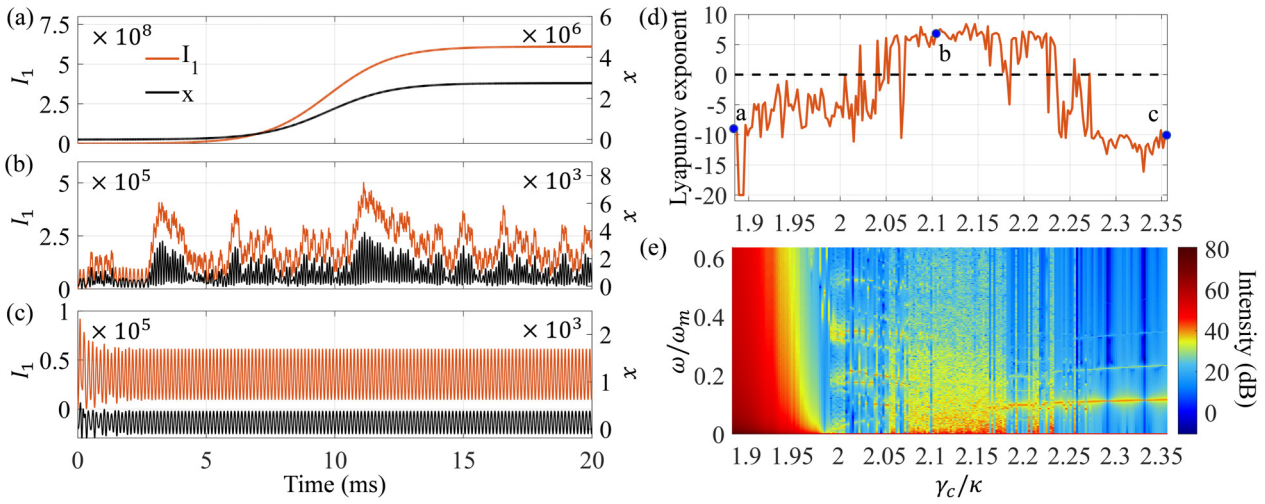

FIG. 2. Evolutions of I_1 (upper) and x (lower) for (a) $\gamma_c \approx 1.88\kappa$, (b) $\gamma_c \approx 2.1\kappa$, and (c) $\gamma_c \approx 2.35\kappa$. (d) Lyapunov exponent of I_1 versus γ_c/κ. (e) Pseudocolormap describes the evolutions of the PSD of I_1 versus ω/ω_m and γ_c/κ. The parameters are $\omega_c = 1216$ THz corresponding to 1550 nm, $\kappa = 8$ kHz, $g = 100$ Hz, $\omega_m/2\pi = 10$ kHz, $\omega_m/2\pi = 1$ kHz, $\omega_c = \omega_d$, $P = 55$ pW, and $\Delta_{\mathrm{Sag}} = 1$ kHz.

because such a coupling approach benefits from the effect of aerodynamic self-adjustment, resulting in robustness against perturbation [47]. In terms of experimental accessibility [48], we select a microcavity with a Q value of approximately 1×10^{10} at a wavelength of 1.55 μm. The coupling between the clockwise and counterclockwise cavity modes is set to be $\kappa = 8$ kHz, which is feasible in the experiments [36], and its value can also be tuned via external scatters experimentally [49]. The mechanical parameters can be flexibly tuned, depending on the requirement of specific experiments. Several well-recognized reviews have exhibited the parameters in various experiments [50–52]. Without loss of generality, we use the integrity with the same order of magnitude as mechanical parameters to simplify the calculation, where the oscillation frequency $\omega_m/2\pi = 10$ kHz [53] and radiative decay rate $\gamma_m/2\pi = 1$ kHz [54]. The coupling between the optical and mechanical modes takes $g = 100$ Hz [53]. We set Δ_{Sag} ranging from 1 to 9 kHz, corresponding to a spinning angular velocity of 40–374 Hz calculated following Ref. [38] using a refractive index of 1.44, a microcavity radius of 50 μm, and a wavelength of 1.55 μm.

III. RESULT AND DISCUSSION

A. Pseudolaser and loss-induced chaos

The dynamics of the light field are characterized by various decay rates of the microcavity in Figs. 2(a)–2(c). We merely show I_1 as I_2 nearly overlaps with I_1. When $\gamma_c \sim 1.88\kappa$, the decay rate of the microcavity is extremely weak. Hence, light intensity accumulation in the microcavity is available in the situation without gain, which corresponds to the positive imaginary part of the eigenvalue [34]. The rapid increase of the light intensity appears initially, which is similar to the general laser generation, as shown in Fig. 2(a). Here we call such light intensity evolution a pseudolaser to distinguish it from a general laser. When the decay rate of the microcavity increases to $\gamma_c \sim 2.1\kappa$, chaos is immediately generated in both the optical and mechanical modes, as shown in Fig. 2(b). By comparing Figs. 2(a) and 2(b), we see that this anti-$\mathcal{PT}$ system produces chaos if the loss is greater, which presents a remarkable distinction from the conventional power-induced chaos.

As usual, a larger positive γ_c results in a faster light decaying in the microcavity and eliminates the chaotic dynamics; in contrast, a negative γ_c generates a laser, and the powerful light strength eventually triggers chaos. For example, in the coupled $\mathcal{PT}$ microcavities, the $\mathcal{PT}$-symmetry-breaking phase allows the gain microcavity to produce power in the system. The ever-increasing light intensity results in an adequate nonlinear interaction from the OMS and finally triggers chaos [13]. However, the chaotic mechanism in the anti-$\mathcal{PT}$ microcavity is distinct from the $\mathcal{PT}$ microcavities. The chaos generation in the anti-$\mathcal{PT}$ microcavity relies on the light strength accumulation from the input instead of the gain in the $\mathcal{PT}$ microcavities.

Such a uniqueness features several interesting dynamics, including the chaotic dynamics. For example, since the anti–$\mathcal{PT}$-symmetric phase produces the pseudolaser when γ_c takes a small positive value, the nonlinear interaction given by the interaction between light and the OMS is negligible compared to that of light intensity. Therefore, the ever-increasing optical strength at the anti–$\mathcal{PT}$-symmetric phase immediately produces the mechanical motion accessing the steady states instead of chaos, as shown in Fig. 2(a). When the decay rate γ_c increases until all imaginary parts of eigenvalues are less than zero in Fig. 1(b), the microcavity accumulates a relatively low light intensity, but its value is comparable to the mechanical movement. The mechanical motion driven by light generates a matching nonlinear interaction on the optical modes. As a result, a comparable light strength with the mechanical movement will more easily form chaos, as shown in Fig. 2(b).

However, achieving chaotic dynamics by continuously increasing the loss γ_c is impossible. For example, when γ_c increases to 2.35κ, the chaotic dynamics vanish, as shown in Fig. 2(c). To evaluate the contribution of γ_c in chaos generation, we plot the Lyapunov exponent

from $\gamma_c \sim 1.88\kappa$ to $\gamma_c \sim 2.35\kappa$ in Fig. 2(d). The Lyapunov exponent is defined by the logarithmic slope of the perturbation $\delta I_1 = |a_1 + \delta a_1|^2 - |a_1|^2$ versus time [13], which mathematically characterizes the rate of separation of trajectories with an infinitesimally close initial condition. To obtain the Lyapunov exponent, we set the perturbation $|\delta a_1|/|a_1| = 10^{-9}$ in the numerical simulations. The positive Lyapunov exponent suggests that the chaotic emission happens, e.g., γ_c takes values from approximately 2.05κ to approximately 2.2κ. Then the evolution of the power spectral density (PSD) further verifies the intriguing loss-induced chaos, as shown in Fig. 2(e). When γ_c/κ is small, the PSD presents a continuous distribution in the broad spectrum, which indicates the fluent pseudolaser dynamics. With the continual growth of γ_c/κ, the chaotic emission appears and yields a broadly discrete distribution. When the loss of the microcavity is beyond the critical value, the PSD collapses to several specific spectrum components, indicating the periodic dynamics. This loss-induced chaos shows that although an ultralow decay rate (or ultrahigh-Q value) of a microcavity is regularly a goal in most scientific areas, it is unfavorable to this proposed chaotic generation design. Consequently, the mechanism of loss-induced chaos may potentially benefit the microcavity fabrication in the chaotic light source.

B. Tunable and switchable chaotic light source

A switchable chaotic light source keeps traffic among the devices on the same network. The tunable rotational speed of the microcavity allows us to control the anti–$\mathcal{PT}$-symmetric and anti–$\mathcal{PT}$-symmetric breaking phases, which offers a genuine opportunity to switch the chaotic emission. As shown in Figs. 3(a) and 3(b), when the rotational speed remains low, the eigenmodes are anti-$\mathcal{PT}$ symmetric and therefore the bifurcation diagrams of I_1 and I_2 feature a bandpass chaotic emission. With the increase of Δ_{Sag}, the eigenmodes enter the anti–$\mathcal{PT}$-symmetric breaking phase and result in a split of their corresponding bifurcation diagrams, as shown in Figs. 3(e)–3(j). The distinguishable bifurcation diagram around resonance indicates that the chaotic emissions switched off near resonance. In addition, such variable multi-bandpass chaos demonstrates that the chaotic bandwidth is tunable by adjusting the microcavity spinning.

The bifurcation diagrams of I_1 and I_2 present a remarkable asymmetry for the opposite detuning, as shown in Fig. 3(a). When $(\omega_c - \omega_d)/\omega_m < 0$, the increment of $\omega_c - \omega_d$ forms a cascade of period-doubling bifurcations, and such a self-similar pattern eventually accesses chaos. In contrast, when $(\omega_c - \omega_d)/\omega_m > 0$, the dynamics of I_1 and I_2 accesses chaos quickly as $\omega_c - \omega_d$ decreases. Physically, the asymmetric bifurcation diagram originates from asymmetric radiation pressure in different wavelengths. To further characterize the asymmetric bifurcation diagrams, we calculated two trajectories of the mechanical motion in phase space with the opposite detuning $\omega_d = \omega_c - 0.4\omega_m$ (left) and $\omega_d = \omega_c + 0.4\omega_m$ (right), as shown in Fig. 3(a). The x and p of the mechanical mode generate a more intensive response if the input has a greater angular frequency. Such an asymmetric nonlinear response of the mechanical mode presents direct evidence to identify the asymmetric radiation pressure triggering the asymmetric optical response.

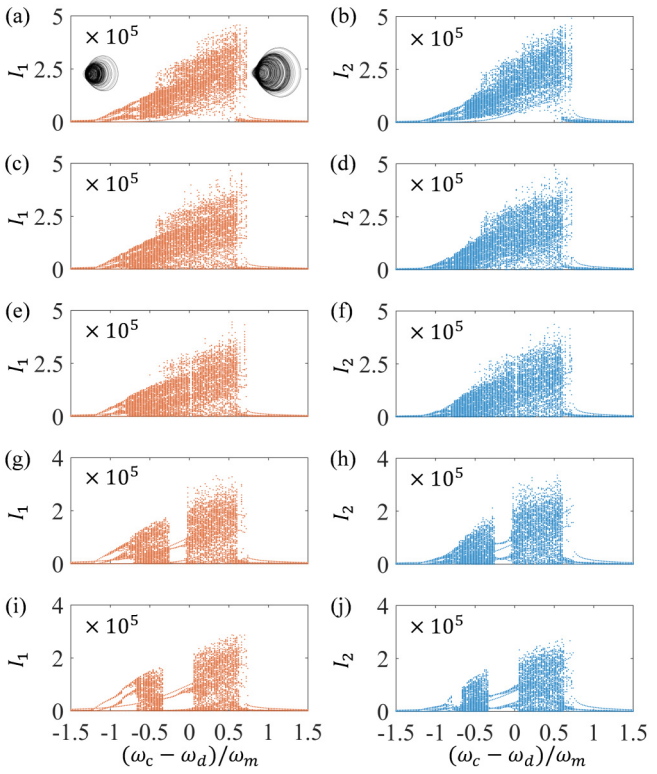

FIG. 3. Bifurcation diagrams of I_1 and I_2 versus $(\omega_c - \omega_d)/\omega_m$ for (a) and (b) $\Delta_{\mathrm{Sag}} = 5.8$ kHz, (c) and (d) $\Delta_{\mathrm{Sag}} = 6.5$ kHz, (e) and (f) $\Delta_{\mathrm{Sag}} = 7$ kHz, (g) and (h) $\Delta_{\mathrm{Sag}} = 8$ kHz, and (i) and (j) $\Delta_{\mathrm{Sag}} = 9$ kHz. The insets in (a) show two trajectories of the mechanical motion at $\Delta_{\mathrm{Sag}} = 5.8$ kHz in phase space with the opposite detuning $\omega_c - \omega_d = \mp 0.4\omega_m$ and $\gamma_c \approx 1.57\gamma$.

C. Two chaotic emissions from one microcavity and reduced chaos threshold

The asymmetric bifurcation diagram due to the nonlinear interaction has sparked curiosity in exploring the intrinsic chiral symmetry of a spinning microcavity anti-$\mathcal{PT}$ system. We apply the Sagnac frequency shift $\Delta_{\mathrm{Sag}} = 8$ kHz to spinning the microcavity and set the power to 120 pW. After that, we input the laser unidirectionally and observe the light field dynamics in the microcavity. When the light with $\omega_d = \omega_c - 0.5\omega_m$ [Figs. 4(a)–4(c)] comes from port A only, I_1 and I_2 generate the chaotic dynamics, as shown in Fig. 4(a); however, when the light with the same angular frequency comes from port B, both I_1 and I_2 reach steady states, as shown in Fig. 4(b). Very interestingly, owing to the asymmetric nonlinear interaction, the reversed chaotic isolation can be found at the opposite detuning $\omega_d = \omega_c + 0.3\omega_m$ [Figs. 4(d)–4(f)], as shown in Figs. 4(d) and 4(e). For a spinning microcavity, the nonreciprocal response is expected because of its asymmetric configuration.

However, if the lights are incident bidirectionally, the microcavity can simultaneously generate two independently chaotic lights from ports A and B, as shown in Figs. 4(c) and 4(f). The chaotic isolation disappears because the optome-

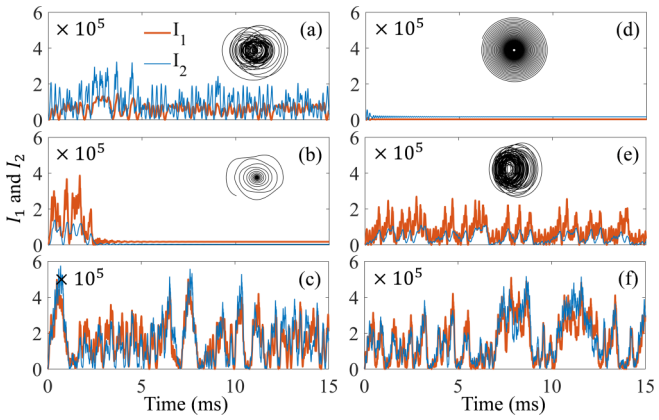

FIG. 4. Evolutions of I_1 (thicker line) and I_2 (thinner line) with the incident direction of input from (a) and (d) port A, (b) and (e) port B, and (c) and (f) both ports, for $\Delta_{\text{Sag}} = 8$ kHz and detunings of (a)–(c) $\omega_d = \omega_c - 0.5\omega_m$ and (d)–(f) $\omega_d = \omega_c + 0.3\omega_m$. The insets in (a), (b), (d), and (e) show the corresponding trajectories of the mechanical motion in phase space.

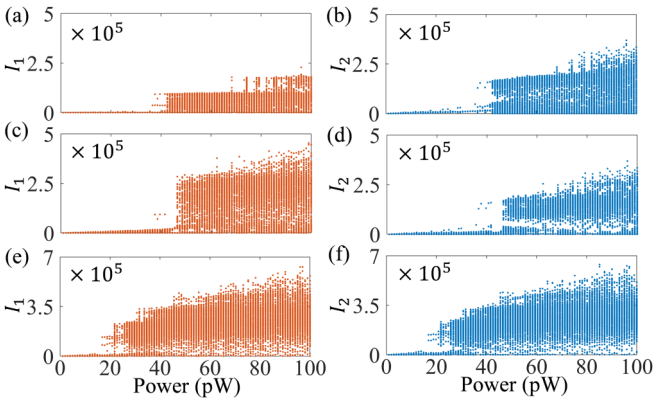

FIG. 5. Bifurcation diagrams of I_1 and I_2 versus power P when light is incident from (a) and (b) port A, (c) and (d) port B, and (e) and (f) both ports, for a detuning of $\omega_d = \omega_c - 0.5\omega_m$.

chanically mediated chaos transfers between two optical fields such that they follow a similar route to chaos (comparing the left and right columns in Fig. 3) but different chaotic dynamics, promising multiplex photonic devices.

Moreover, the arrangement of bidirectional light input provides an extra advantage of the reduced chaos threshold. When the light is incident from either port A or B, the bifurcation diagrams of I_1 and I_2 show a similar chaos threshold at approximately 50 pW, as shown in Figs. 5(a)–5(d). In contrast, when the inputs come from ports A and B, the chaos threshold dramatically decreases to approximately 20 pW, as shown in Figs. 5(e) and 5(f). The arrangement of two-port light input enables us to generate two chaotic lights using the same amount of energy as the unidirectional light input. Such a high-efficiency chaotic light source arrangement is desirable in space-starved silicon on-chip applications.

IV. CONCLUSION

In summary, this study proposed a tunable chaotic light source in the spinning anti–$\mathcal{PT}$-symmetric and anti–$\mathcal{PT}$-symmetric breaking OMS. Unlike earlier chaotic light sources, the continuously tuned rotational speed enables us to control the anti-$\mathcal{PT}$ phase transition and then freely switch the bandpass–band-stop chaotic emission in a tunable bandwidth. In additioin, several phenomena were discovered, such as loss-induced chaos and a chiral input reduced chaos threshold. This chaos generation mechanism was identified in the spinning microcavity anti-$\mathcal{PT}$ OMS. This study provides a continuous tunable chaotic sources scheme and offers a platform further to exploit the benefits of non-Hermitian optics and chaotic dynamics.

ACKNOWLEDGMENTS

We are grateful for financial support from the Fundamental Research Funds for the Central Universities (Grant No. 21620328) the National Natural Science Foundation of China (Grants No. 61805108, No. 61904067, and No. 62075088), and the Guangdong Basic and Applied Basic Research Foundation (Grants No. 2020A1515011498 and No. 2017A010101013).

[1] T. Carmon, H. Rokhsari, L. Yang, T. J. Kippenberg, and K. J. Vahala, Phys. Rev. Lett. **94**, 223902 (2005).
[2] T. Carmon, M. C. Cross, and K. J. Vahala, Phys. Rev. Lett. **98**, 167203 (2007).
[3] L. Bakemeier, A. Alvermann, and H. Fehske, Phys. Rev. Lett. **114**, 013601 (2015).
[4] G.-Q. Qin, M. Wang, J.-W. Wen, D. Ruan, and G.-L. Long, Photon. Res. **7**, 1440 (2019).
[5] J. Ma, C. You, L.-G. Si, H. Xiong, J. Li, X. Yang, and Y. Wu, Phys. Rev. A **90**, 043839 (2014).
[6] L. Qi, G.-L. Wang, S. Liu, S. Zhang, and H.-F. Wang, Opt. Lett. **45**, 2018 (2020).
[7] Y.-X. Zeng, J. Shen, M.-S. Ding, and C. Li, Opt. Express **28**, 9587 (2020).
[8] C.-H. Bai, D.-Y. Wang, S. Zhang, S. Liu, and H.-F. Wang, Adv. Quantum Technol. **4**, 2000149 (2021).
[9] E. E. Wollman, C. U. Lei, A. J. Weinstein, J. Suh, A. Kronwald, F. Marquardt, A. A. Clerk, and K. C. Schwab, Science **349**, 952 (2015).
[10] Y. Jiang, S. Maayani, T. Carmon, F. Nori, and H. Jing, Phys. Rev. Appl. **10**, 064037 (2018).
[11] Z.-X. Liu, C. You, B. Wang, H. Dong, H. Xiong, and Y. Wu, Nanoscale **12**, 2118 (2020).
[12] W. Chen, J. Zhang, B. Peng, Ş. K Özdemir, X. Fan, and L. Yang, Photon. Res. **6**, A23 (2018).
[13] X.-Y. Lü, H. Jing, J.-Y. Ma, and Y. Wu, Phys. Rev. Lett. **114**, 253601 (2015).

[14] F. Monifi, J. Zhang, Ş. K. Özdemir, B. Peng, Y.-x. Liu, F. Bo, F. Nori, and L. Yang, Nat. Photon. **10**, 399 (2016).
[15] Z. Zheng, Y. Zhang, M. Huang, Z. Chen, S. Yu, and H. Guo, Opt. Express **28**, 22388 (2020).
[16] J. Wang, F. Sciarrino, A. Laing, and M. G. Thompson, Nat. Photon. **14**, 273 (2020).
[17] C. Abellan, W. Amaya, D. Domenech, P. Muñoz, J. Capmany, S. Longhi, M. W. Mitchell, and V. Pruneri, Optica **3**, 989 (2016).
[18] L. Wang, X. Mao, A. Wang, Y. Wang, Z. Gao, S. Li, and L. Yan, Opt. Lett. **45**, 4762 (2020).
[19] X. Jiang, L. Shao, S.-X. Zhang, X. Yi, J. Wiersig, L. Wang, Q. Gong, M. Lončar, L. Yang, and Y.-F. Xiao, Science **358**, 344 (2017).
[20] M. Arnal, G. Chatelain, M. Martinez, N. Dupont, O. Giraud, D. Ullmo, B. Georgeot, G. Lemarié, J. Billy, and D. Guéry-Odelin, Sci. Adv. **6**, eabc4886 (2020).
[21] M. Zhang, C. Wang, Y. Hu, A. Shams-Ansari, T. Ren, S. Fan, and M. Lončar, Nat. Photon. **13**, 36 (2019).
[22] D. P. Lake, M. Mitchell, B. C. Sanders, and P. E. Barclay, Nat. Commun. **11**, 2208 (2020).
[23] A. Bergman, R. Duggan, K. Sharma, M. Tur, A. Zadok, and A. Alù, Nat. Commun. **12**, 486 (2021).
[24] Z. Shen, C.-H. Dong, Y. Chen, Y.-F. Xiao, F.-W. Sun, and G.-C. Guo, Opt. Lett. **41**, 1249 (2016).
[25] H. Jing, S. K. Özdemir, X.-Y. Lü, J. Zhang, L. Yang, and F. Nori, Phys. Rev. Lett. **113**, 053604 (2014).
[26] J. Zhang, B. Peng, Ş. K. Özdemir, K. Pichler, D. O. Krimer, G. Zhao, F. Nori, Y.-x. Liu, S. Rotter, and L. Yang, Nat. Photon. **12**, 479 (2018).
[27] Q.-T. Cao, R. Liu, H. Wang, Y.-K. Lu, C.-W. Qiu, S. Rotter, Q. Gong, and Y.-F. Xiao, Nat. Commun. **11**, 1136 (2020).
[28] B. Peng, Ş. K. Özdemir, S. Rotter, H. Yilmaz, M. Liertzer, F. Monifi, C. M. Bender, F. Nori, and L. Yang, Science **346**, 328 (2014).
[29] X. Mao, G.-Q. Qin, H. Yang, H. Zhang, M. Wang, and G.-L. Long, New J. Phys. **22**, 093009 (2020).
[30] F. Klauck, L. Teuber, M. Ornigotti, M. Heinrich, S. Scheel, and A. Szameit, Nat. Photon. **13**, 883 (2019).
[31] S. Weimann, M. Kremer, Y. Plotnik, Y. Lumer, S. Nolte, K. G. Makris, M. Segev, M. C. Rechtsman, and A. Szameit, Nat. Mater. **16**, 433 (2017).
[32] L. Ge and H. E. Türeci, Phys. Rev. A **88**, 053810 (2013).
[33] S. Ke, D. Zhao, J. Liu, Q. Liu, Q. Liao, B. Wang, and P. Lu, Opt. Express **27**, 13858 (2019).
[34] Y. Yang, Y.-P. Wang, J. W. Rao, Y. S. Gui, B. M. Yao, W. Lu, and C.-M. Hu, Phys. Rev. Lett. **125**, 147202 (2020).
[35] Y. Li, Y.-G. Peng, L. Han, M.-A. Miri, W. Li, M. Xiao, X.-F. Zhu, J. Zhao, A. Alù, S. Fan, and C.-W. Qiu, Science **364**, 170 (2019).
[36] Y.-H. Lai, Y.-K. Lu, M.-G. Suh, Z. Yuan, and K. Vahala, Nature (London) **576**, 65 (2019).
[37] B. Lu, X.-F. Liu, Y.-P. Gao, C. Cao, T.-J. Wang, and C. Wang, Opt. Express **27**, 22237 (2019).
[38] H. Zhang, R. Huang, S.-D. Zhang, Y. Li, C.-W. Qiu, F. Nori, and H. Jing, Nano Lett. **20**, 7594 (2020).
[39] F. Zhang, Y. Feng, X. Chen, L. Ge, and W. Wan, Phys. Rev. Lett. **124**, 053901 (2020).
[40] H. Jing, H. Lü, S. K. Özdemir, T. Carmon, and F. Nori, Optica **5**, 1424 (2018).
[41] W. Lin, H. Zhang, Z. Gong, B. Liu, H. Liu, B. Song, and J. Wu, J. Lightw. Technol. **39**, 2443 (2021).
[42] I. M. Mirza, W. Ge, and H. Jing, Opt. Express **27**, 25515 (2019).
[43] H. Shi, Z. Xiong, W. Chen, J. Xu, S. Wang, and Y. Chen, Opt. Express **27**, 28114 (2019).
[44] R. Huang, A. Miranowicz, J.-Q. Liao, F. Nori, and H. Jing, Phys. Rev. Lett. **121**, 153601 (2018).
[45] B. Li, R. Huang, X. Xu, A. Miranowicz, and H. Jing, Photon. Res. **7**, 630 (2019).
[46] W. S. Xue, H. Z. Shen, and X. X. Yi, Opt. Lett. **45**, 4424 (2020).
[47] S. Maayani, R. Dahan, Y. Kligerman, E. Moses, A. U. Hassan, H. Jing, F. Nori, D. N. Christodoulides, and T. Carmon, Nature (London) **558**, 569 (2018).
[48] V. Huet, A. Rasoloniaina, P. Guillemé, P. Rochard, P. Féron, M. Mortier, A. Levenson, K. Bencheikh, A. Yacomotti, and Y. Dumeige, Phys. Rev. Lett. **116**, 133902 (2016).
[49] W. Chen, Ş. K. Özdemir, G. Zhao, J. Wiersig, and L. Yang, Nature (London) **548**, 192 (2017).
[50] C. Dong, Y. Wang, and H. Wang, Natl. Sci. Rev. **2**, 510 (2015).
[51] M. Metcalfe, Appl. Phys. Rev. **1**, 031105 (2014).
[52] M. Aspelmeyer, T. J. Kippenberg, and F. Marquardt, Rev. Mod. Phys. **86**, 1391 (2014).
[53] D. Kleckner, B. Pepper, E. Jeffrey, P. Sonin, S. M. Thon, and D. Bouwmeester, Opt. Express **19**, 19708 (2011).
[54] R. Pennetta, S. Xie, R. Zeltner, J. Hammer, and P. S. J. Russell, Photon. Res. **8**, 844 (2020).